Multiscale analysis of tire and asphalt pavement interaction via coupling FEM–DEM simulation

Haitao Ge, Juan Carlos Quezada, Vincent Le Houerou, Cyrille Chazallon

Multiscale Analysis of Tire and Asphalt Pavement Interaction Via Coupling FEM-DEM Simulation

Haitao Ge[a,*], Juan Carlos Quezada[a], Vincent Le Houerou[b], Cyrille Chazallon[a,c]

[a] *Université de Strasbourg, INSA de Strasbourg, CNRS, ICube, UMR 7357, F-67000 Strasbourg France*
[b] *Université de Strasbourg, CNRS, ICube, UMR 7357, F-67000 Strasbourg, France*
[c] *Laboratory of Rd. and Traffic Engineering, Shandong Jianzhu University, Jinan, People's Republic of China*

Abstract

With the aging of roads and the lack of resources for maintenance, a thorough understanding of the interaction between tires and asphalt pavements is crucial to optimize asphalt pavement surface design. Currently, most research on this interaction system is conducted using mesh-based methods in the frame of continuum mechanics, which are insufficient to model the discontinuity behavior of asphalt mixtures during their lifespan. In this study, the Contact Dynamics method is introduced to investigate this interaction system by coupling the finite element method (FEM) and the discrete element method (DEM). FEM is utilized to model the tire and capture the resulting contact stresses on the pavement surface, while DEM is used to model the heterogeneous structure of an asphalt mixture and examine internal mixture responses at the particle scale. Analysis of contact stress distributions for free-rolling and full-braking conditions proves the tire model's effectiveness. According to particle displacement and force distributions, particles tend to flow along the longitudinal direction and undergo a high tangential contact force under full-braking compared with

*Corresponding author
Email address: haitao.ge@etu.unistra.fr (Haitao Ge)

those under free-rolling, resulting in mixture instability and damage initiation. This study offers an enriching supplement and expansion to mesh-based methods for analyzing pavement surface degradation under tire loads, which can provide insight into pavement surface design.

Keywords: Tire-pavement interaction, Contact dynamics method, Multiscale approach, Finite element modeling, Discrete element modeling, Non-uniform tire load

1. Introduction

In a context where road networks are aging, and where resources for maintenance of these networks are decreasing, it is essential to study the tire and asphalt pavement interaction deeply in order to determine the failure mechanisms in surface deterioration and thus optimize their formulation and service. In the conventional pavement design method, for the sake of simplicity, tire loads are assumed as normal to the rolling surface and uniform [1, 2, 3]. Experiments have shown, however, that the real tire load is not uniform and that the stress distribution is not normal to the rolling surface since both vertical and tangential contact stresses are generated at the tire-pavement interface [4, 5, 6]. There exists much research proving that the actual tire load induces quite different pavement responses, compared to the conventional uniform load [7, 8, 9], especially in terms of pavement surface degradation and near-surface crack development [10].

The tire-pavement interaction is an extremely complex contact problem. Experimental measurements are arduous because of their time-consuming and expenses and limitations in studying various boundary conditions of this interaction system. On the other hand, numerical tools provide an effective way to explore this system while taking into account the system complexity. Wang et al. [6] investigated the effects of tire types on pavement responses at the

near-surface position and provided a reference for the truck tire optimization. They also validated the non-uniformity of tire contact stresses and localized tangential contact stresses based on the finite element method (FEM) [11]. Guo et al. [12, 13] analyzed the contact stress distribution of a bus tire on the pavement using FEM, various tire work conditions were found to affect critical slip ratios and rolling resistance. Wollny et al. [14, 15] proposed a strategy to simulate a rolling tire on the pavement surface based on FEM and indicated that tire rolling conditions have significant effects on the macroscopic pavement performance. To reduce the cost of FEM computation, Manyo et al. [16, 17] proposed a fast tire-pavement modeling method using the semi-analytical method (SAM) and studied pavement responses under different tire rolling conditions. They found that the maximum tensile strains caused by tire edges could lead to top-down cracking. Oubahdou et al. [18] studied tire contact stresses under various tire inclinations by combing SAM and sensor measurements, significant shear stresses were observed on the pavement surface as a result of tire turnings.

However, current research has primarily focused on macro simulations of the tire-pavement interaction, in which the asphalt pavement is usually assumed homogeneous due to the limitation of mesh-based methods in the continuum mechanics framework such as FEM and SAM. Actually, asphalt mixtures are complex multi-phase systems composed of aggregate particles and asphalt mastic. Mesh-based methods can simulate tire contact stresses precisely on the pavement surface, but it is still a struggle to quantify internal mixture responses at the particle scale.

Due to the heterogeneous structure of asphalt mixtures, the discrete element method (DEM) has been widely adopted in the last decades as a complementary alternative for classical mesh-based methods. A variety of studies have been conducted using DEM to investigate the micromechanical behavior of asphalt

mixtures. In order to simulate aggregates and asphalt mastic, a micro-fabric discrete element modeling approach was early developed based on linear elastic contact models [19]. Afterward, viscoelastic contact models gradually became widely used by researchers to model asphalt mastic [20, 21, 22],in order to evaluate the dynamic modulus [23, 24], creep [25] and compaction behavior of asphalt mixtures [26, 27]. For the simulation of tire load effects on asphalt mixtures, Ma et al. [28, 29] performed a 2D (two-dimensional) simulation for the wheel tracking test based on DEM. Xue et al. [30] and Wang et al. [31] extended the virtual wheel tracking test in 3D simulation via DEM. However, current DEM models concentrated on the simulation of asphalt mixture samples in laboratory tests due to the limitation of computation costs, moreover the boundary loading conditions applied in most simulations are usually uniform and simplified. Research on the simulation of non-uniform tire loads on asphalt pavement via DEM models, to the best of our knowledge, is rare.

A number of studies have been conducted to explore the interaction between unbound materials and tires using multiscale simulations [32, 33, 34]. However, the current research mainly focuses on the simulation of unbound materials such as sands, soils, and gravels. The contact laws used are mainly frictional and the particle shape is usually limited to spheres because of computation costs. Moreover, the road surface made with unbound materials is relatively soft compared to the asphalt pavement surface, which leads to different tire contact stress distributions on these two kinds of road surfaces. Considering the viscoelastic nature and irregular particle shapes in an asphalt mixture, the current coupling simulation methods are inadequate for simulating asphalt pavement and tire interaction. Consequently, a new coupling framework dedicated to the interaction system between the tire and the asphalt pavement surface is required.

Herein, we report a multiscale simulation method to examine the tire-pavement

interaction combining FEM and DEM approaches based on the contact dynamics (CD) method. The multiscale modeling approach brings the benefit that FEM can provide precise tire contact stresses on the pavement surface, while DEM can evaluate effectively the internal discontinuity behavior of the asphalt mixture. This method proposes an innovative and promising way to simulate the tire-pavement interaction and to reveal degradation mechanisms of the asphalt pavement surface under different tire loads at the particle scale.

2. Contact modeling theory

Tire-pavement interaction is a typical contact problem in the contact mechanics domain. In computational contact mechanics, the contact problem is an extremely non-linear, non-smooth, and non-differential problem. A unilateral contact problem can be modeled using Signorini's condition and Coulomb's friction law (Figure 1). As seen here, the contact conditions are essentially infinite steep, which makes them non-differentiable.

For a classical solution to the contact problem, the reaction force (R) is defined as a function of the gap (g), where g represents the penetration of two contacting surfaces. The relation between g and R can instead be replaced with steep mapping graphs and thus be solved by non-linear differential equations. Replacing the infinite steep formulation with some smooth relations could be considered mathematically as a regularization or numerically as a penalty method. With this strategy, contact conditions are modeled as a sequence of steep laws using regularization techniques, and the nonlinear laws being thus handled by means of an explicit time integrator. It is adopted widely for solving contact problems in FEM [35] and explicit smooth DEM simulations pioneered by P. Cundall [36, 37] because of its simplicity and easy implementation in numerical algorithms.

There are, however, some weaknesses to this method from its principles: 1) The time step is mandatory small in order to ensure the calculation stability, especially when dealing with high contact stiffness; 2) Damping must be introduced, either through the contact laws or as a numerical trick, to ensure the stability of explicit schemes. 3) The equilibrium state is hard to achieve via an explicit method when considering the tangential friction force. 4) Penetration is inevitable. The constraint condition is satisfied precisely when the penalty parameter tends to infinity. However, the resulting equations could be ill-conditioned if the penalty parameter is too large and thus choosing the relevant parameters could be tricky;

Differently, Jean-Jacques Moreau developed the Non-smooth Contact Dynamics method (NSCD), shortly Contact dynamics (CD) in 1984 for the implicit non-smooth interaction model [38] and this method has proved to be an effective tool for modeling a large number of contacting rigid or deformable bodies [39, 40, 41]. Unlike the method described above, the CD method uses non-differential steep laws to define the relationship between relative velocities U and impulses I. Signorini's condition and Coulomb's friction law are cited as the foundation of contact laws. Figure 1 compares the CD method and the classical penalty method for solving contact conditions.

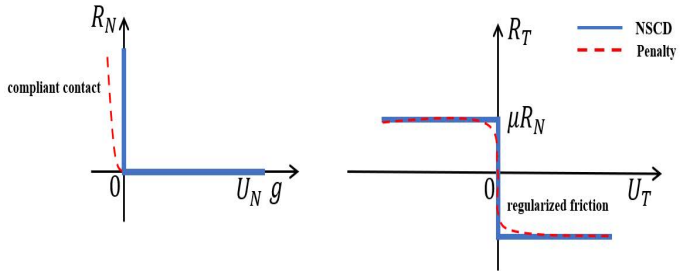

Figure 1: Comparison between the two contact modeling methods: Normal (left) and Tangential (right)

At the local frame, the contact management between two objects is based

on the so-called candidate/antagonist approach (Figure 2). According to this approach, it is assumed that one is able to define for each point (C) of the candidate boundary its (unique) nearest point (A) on the antagonist boundary, a local reference frame $(\mathbf{n}, \mathbf{t}, \mathbf{s})$ attached to the antagonist body is defined at the contact point A. For deformable objects, one has to consider contact elements composed of a node versus the discretized antagonist face boundaries.

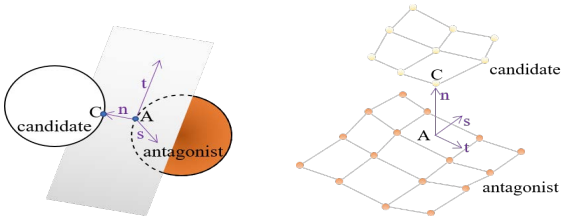

(a) Rigid bodies (b) Deformable bodies

Figure 2: Candidate/antagonist approach

The contact laws are managed with an implicit method using a Non-Linear Gauss-Seidel algorithm (NLGS) at each time step. Kinematic constraints arising from contacts are calculated simultaneously by combining them with dynamics equations, in order to determine all the velocities and contact forces in the system. Furthermore, the regularized parameters such as damping are removed from the local contact frame. As a result, the implicit method can be used to find equilibrium states more accurately than explicit methods [42]. In comparison to explicit DEMs, the CD method allows using larger time steps since it determines the characteristic system time of particle dynamics.

As shown schematically in Figure 3, three main types of contact may occur between two polyhedral particles: point contact, line contact, and surface contact. The line (edge–face) contacts can be modeled by two points, while three points can model surface (face-face) contacts since they involve equal geometric unilateral constraints between the two faces. There are several steps involved in the determination of the contacts between two polyhedral particles. In the first

step, we compute a list of neighboring pairs using a "bounding box" method. Then, an overlap calculation is done for each pair, using the "common plane" method. [43]. Contact planes are determined by their intersection in the case of an overlap. This detection method allows simulating large samples composed of polyhedral particles in a relatively short time [44, 45]. Finally, for each potential contact point, the local impulsion and velocity are calculated independently, and the resultant force is then assigned to the contact.

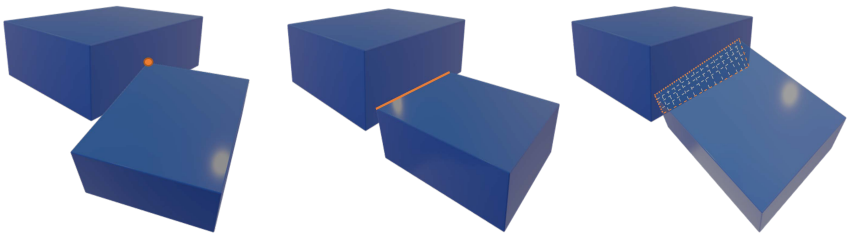

(a) Point contact (b) Line contact (c) Surface contact

Figure 3: Contact situations that may occur between two polyhedral particles

Considering its advantages, we used the CD method to simulate the tire-pavement surface interaction and aggregate particles in asphalt mixtures. The open-source software LMGC90 (`https://git-xen.lmgc.univ-montp2.fr/lmgc90/lmgc90_user/-/wikis/home`) is adopted in which CD method is built-in.

3. Tire modeling and calibration

3.1. Tire structure and model construction

The tire structure is extraordinarily complex. For a typical radial tire, it comprises components at several scales such as ribs, grooves, beads, sidewalls, and belt piles, and every part has its own material properties. Numerical simulations have a universal purpose of capturing the main features of a problem and ignoring its secondary factors. A wheel can be divided into two parts from

the point of its functionality: a deformable part that models the tire itself and air together, which interacts with the pavement surface directly, and a rigid rim serving as the driven system following the tire motion that supports the loading, and transmits acceleration and braking. We adopted this strategy in tire modeling for its efficiency and simplicity.

In the modeling, a passenger tire (185/65R15) was chosen and a three-dimensional laser scanner (FARO Freestyle3D) was employed to reconstruct the tire geometry (Figure 4).

(a) Laser scanning (b) Rendering

Figure 4: Tire scanning process

After the scanning procedure, the open-source software Meshlab (`https://www.meshlab.net/`) was used to process the cloud points and reconstruct the tire shape. Raw tire data are very noisy and have many textures, which are not conducive to numerical simulation since it produces geometrical non-linear complexity. The tire data were handled based on a method proposed elsewhere [46]. Based on the scanning results, the longitudinal tire grooves were retained, whereas the transverse textures were omitted by image processing, and the rigid rim part was replaced for the sake of simplicity by a cylinder inheriting the same diameter. Then, the open-source software Gmsh (`https://gmsh.info/`) was used to conduct the meshing process. A fine mesh ($5mm$

characteristic length) was defined for the outer tire part and a coarse one was chosen for the inner tire part (30mm characteristic length) to achieve a good precision while saving the computation time. Figure 5 shows the generated tire model.

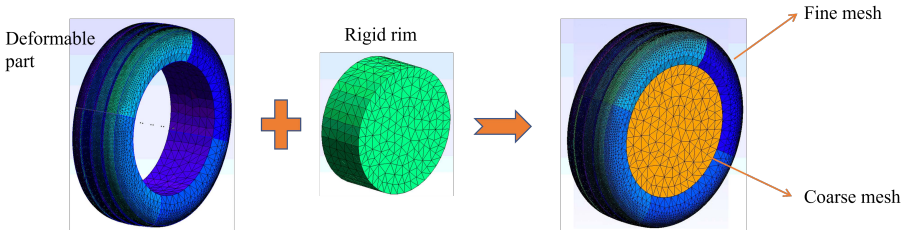

Figure 5: Tire model and mesh refinement

3.2. Model calibration

The rim part was assumed to be rigid, and the deformable part was modeled via a linear elastic material. The degree of freedom of these two objects was fixed by setting a coupled contact law so that the deformable and rigid parts can stick together and prevent sliding. To identify elasticity parameters of the deformable part, a tire compression test [47] was performed.

In the experiment, the tire was placed between two rigid plates, the force sensor was set on the top plate. We then recorded the force value (F [N]) and displacement (z [mm]) of the top plate. We measured the displacement values of the top plate at four force levels (F = 1, 2, 3, 4 kN), then the tire load-deflection test results were used furthermore to calibrate the tire bulk behavior through numerical simulations.

During the numerical simulation of the reproduced test, Signorini's condition and Coulomb's friction law were adopted as the contact law between the tire and the rigid plates, and the friction coefficient was set as close to zero considering the slippery feature of the plate surface. A numerical top rigid plate was then

subjected to the same vertical velocity as in the experimental test. As a final step, the numerical load-deflection curve of the rigid top plate was recorded during the simulation and then compared with the experimental results. The material properties were altered in the numerical simulation to obtain deflection values close to experimental measurements. Figure 6 presents the compression test process and calibration results, where the tire inflation pressure was equal to 2.2 bar. The predicted load-deflection curve agrees well with the experimental data, the material parameters for the numerical simulation were determined to be Young's modulus of 1.0 MPa and Poisson's ratio of 0.36. It is worth to note that the deformable part is compressible since it models rubber and air together. The nonlinear the load-deflection curve comes from the geometric nonlinearity.

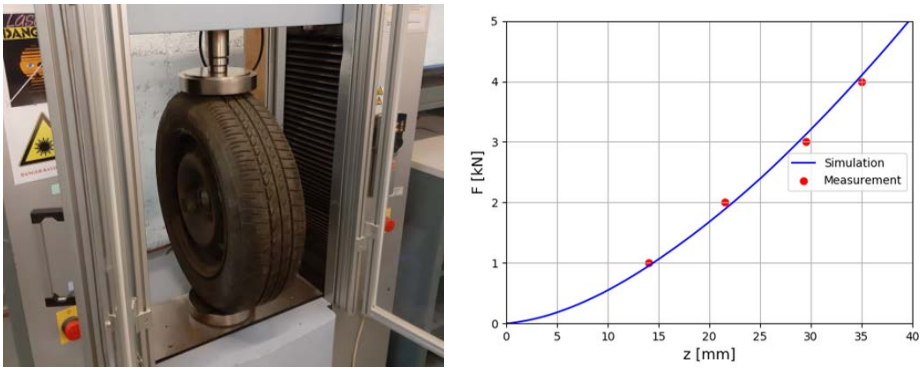

(a) Compression test (b) Load-deflection curve

Figure 6: Comparisons between measured and calculated tire deflections

4. Macro simulation of the tire induced-loading on the pavement surface

4.1. Tire rolling contact model

Pavement surfaces degrade primarily due to traffic loads, where tires are the interface between a vehicle and the road surface. Pavement degradation analysis requires contact stress distributions of a tire on the pavement surface.

Depending on the driving state and direction, a vehicle tire could withstand forces and torques in every directions. Figure 7 illustrates the force status of a rolling tire and the contact mechanical actions transmitted to the pavement surface. The vertical force is given by the weight of the vehicle and depends on the dynamic behavior of the suspension. The longitudinal force is generated when the tire is traveling in a straight line, during acceleration or braking. The side (lateral) force is generated when the tire is changing direction, during cornering.

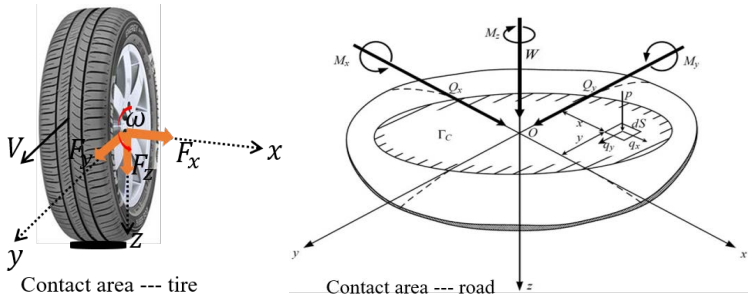

(a) (b)

Figure 7: Tire driven forces during rolling (a) and pavement contact forces (b) [48]

where:

- F_x [N] — lateral tire force.
- F_y [N] — longitudinal tire force.
- F_z [N] — vertical tire force.
- ω [rad/s] — tire angular velocity.
- V [m/s] — tire longitudinal velocity.
- $Q_x,\ Q_y,\ W$ — contact forces on the pavement surface.
- $M_x,\ M_y,\ M_z$ — contact moments on the pavement surface.

The contact stresses on the pavement surface including the normal and tangential parts were solved by the balance formulations below:

$$W = \int_{\Gamma c} p(x,y)dS = F_z \tag{1}$$

$$Q_x = \int_{\Gamma c} q_x(x,y)dS = F_x \tag{2}$$

$$Q_y = \int_{\Gamma c} q_y(x,y)dS = F_y \tag{3}$$

where:

- W [N] — normal load applied.
- Q_x, Q_y [N] — tangential load applied.
- $p(x,y)$ [Pa] — normal contact pressure at a point(x,y).
- $q(x,y)$ [Pa] — tangential contact pressure at a point(x,y).
- Γc [m^2] — contact area.

After the construction of formulations solving the contact problem between the tire and pavement surface, it is possible to study the pavement surface responses under various tire loading conditions.

A pavement surface layer interacting with the tire was built and shown in figure 8. A dimension of 0.3 m×0.3 m×0.04 m in x, y, and z-direction was chosen for the modeling of a typical pavement wearing course. The y-axis represents the tire moving direction, and the x-axis represents the transverse (or lateral) direction, the spatial mesh size was chosen as 5 mm×5 mm×10 mm in x, y and z respectively, the mesh size of the contact zone under the tire matches the mesh size of the tire outer part to capture the stress distribution accurately.

Asphalt mixtures exhibit complex visco-elastic and visco-plastic behaviors in regard to loading conditions mainly including temperature and loading fre-

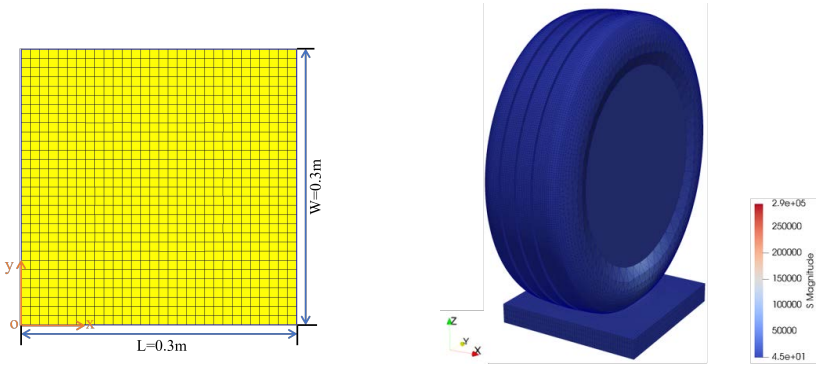

(a) Foundation layer (b) Tire loading on the surface

Figure 8: Asphalt surface layer and tire

quency. For the sake of computation efficiency, the elasticity modulus and Poisson's ratio of the surface layer was chosen to be 13,000 MPa and 0.35 respectively according to the experimental complex modulus test results at 15 °C and 10 Hz [49]. Thus the asphalt mixture was assumed as an elastic material in the modeling [50]. We used Coulomb's friction law to describe the contact between the tire and the pavement surface, and the friction coefficient was chosen as μ=0.8, where this value is commonly used as reference value for tire-pavement friction. For simulating tire axial loads, the driven forces were applied on the rim part of the calibrated tire model. During the entire simulation, the layer bottom was used as a fixed boundary condition.

The weight of a four-wheeled passenger car was assumed to be equally distributed between tires, the vertical load F_z of a tire can then be calculated as follows:

$$F_z = G_v/4 = m_v \cdot g_a/4 \tag{4}$$

Where,

- G_v [N] — vehicle weight.

- m_v — vehicle mass, it was set to 2.0 t in this study.
- g_a — gravitational acceleration ($9.8\ m \cdot s^{-2}$).

In this study, we examined the longitudinal tire behavior, including braking and acceleration. For a rolling tire without cornering, its longitudinal velocity can be calculated as:

$$V_{y0} = r_w \cdot \Omega_0 \tag{5}$$

where:

- V_{y0} [m/s] — rolling tire longitudinal velocity.
- r_w [m] — rolling tire radius.
- Ω_0 [rad/s] — rolling tire angular velocity.

When a torque is applied to the tire, either for acceleration or braking, a longitudinal slip (k) occurs between the tire and the vehicle [51], calculated as:

$$k = \begin{cases} -\dfrac{V_{y0} - r_w \cdot \Omega}{V_{y0}} = -\dfrac{\Omega_0 - \Omega}{\Omega_0}, a_v < 0 \\ \dfrac{r_w \cdot \Omega - V_{y0}}{r_w \cdot \Omega} = -\dfrac{\Omega - \Omega_0}{\Omega}, a_v > 0 \end{cases} \tag{6}$$

where:

- k [-] — longitudinal tire slip.
- Ω [rad/s] — braking/accelerating tire angular velocity.
- a_v [m/s^2] — vehicle acceleration.

During braking, if the tire is completely locked ($\Omega = 0$), the k parameter will reach a minimum value equals to -1. During acceleration, if the vehicle is

activating but the tire is at standstill ($\Omega_0 = 0$), the k parameter reaches its maximum value of 1.

For k different from zero, it corresponds to the acceleration ($k > 0$) or braking ($k < 0$) states, and the tire is subjected to longitudinal forces. For $k = 0$, it corresponds to the free-rolling state. When the tire is rolling in a steady-state (angular and translational velocities are constant), the dynamic process of the tire rolling is time-independent [14]. In the steady-state simulation, there is no requirement for the tire to move over the FEM mesh of the pavement, which makes it possible to calculate this interaction system numerically efficiently. Furthermore, it also allows the use of a dense mesh within the contact area of the pavement and the tire, which allows the accurate capture of tire contact stresses on the pavement surface. The tire loading state during rolling is also determined by the tire rolling speed. According to previous studies, for a passenger tire, the rolling tire radius r_w changes slightly when the tire experiences different rolling speed (from 0 to 5 km/h) [13]; and tire rolling speed (from 15 to 90 km/h) has a negligible effect on the tire contact stresses [52]. Herein, we assume that the tire rolling speed does not affect the tire loading state. Consequently, the tire rolling contact can be considered to be stationary in the steady-state. As declared above, there are therefore two coupled effects: a normal effect caused by vertical loads, and a tangential effect caused by tangential loads (mainly from tire acceleration or braking).

4.2. Tire contact stress distribution under free-rolling

When a tire is in a free-rolling state, only vertical load $F_z = 5\ kN$ acts on the tire. Figure 9a shows the magnitude of tire contact stresses on the pavement surface. This contour shows that the tire-pavement contact area is close to an ellipse. Figure 9b shows that the vertical contact stress is not uniform across the whole contact area. The distribution of the vertical stress is symmetric along

the y-axis (tire length), and the maximum stress values concentrate at the tire center ribs.

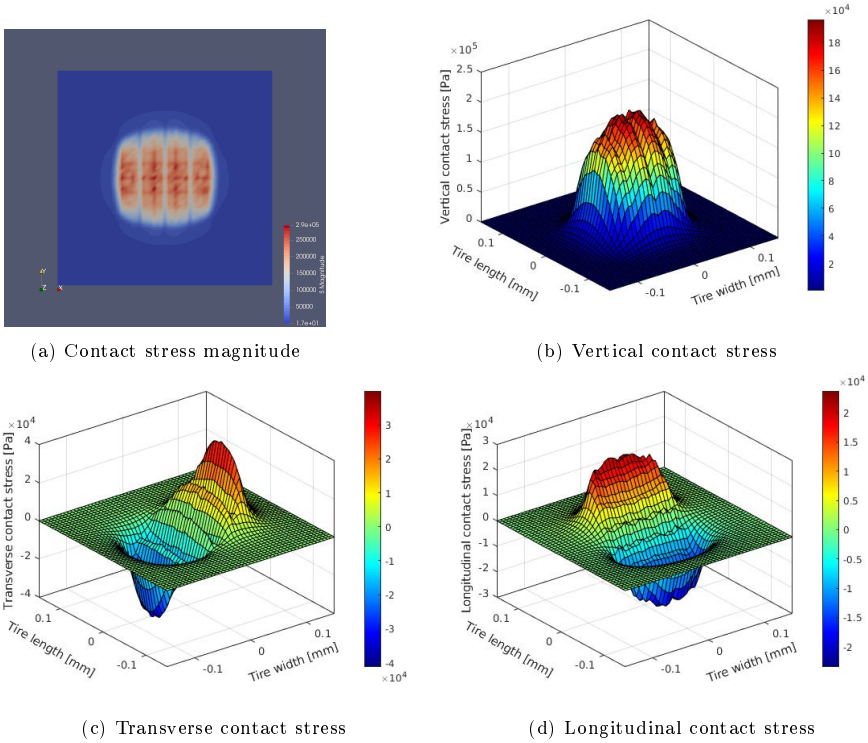

(a) Contact stress magnitude

(b) Vertical contact stress

(c) Transverse contact stress

(d) Longitudinal contact stress

Figure 9: Contact stress distribution contour at free-rolling

Figure 9c and figure 9d demonstrate that the tire also induces contact stress components in lateral and longitudinal directions, affecting pavement responses together. The longitudinal contact stress distributes symmetrically along the y-axis, its peak values locate at the tire center ribs. The lateral contact stress distributes symmetrically along the x-axis (tire width) and the stress values achieve maximum at the tire edge ribs. In terms of peak values, the ratio between vertical, lateral, and longitudinal contact stress is about 1: 0.18: 0.14; the tangential contact stresses are considerably low compared to the vertical contact stress as expected for free-rolling conditions.

4.3. Tire contact stress distribution under full-braking

Since the longitudinal forces associated with a tire are similar for acceleration and braking, this study analysed tire contact stresses in braking conditions. In braking, the direction of the braking torque is opposite to the tire moving direction. If the tire slip reaches its minimum value (k=-1), it means that the tire is fully locked (hence full-braking), and the longitudinal force F_y can then be calculated as follows:

$$F_y = \mu \cdot F_z \tag{7}$$

Where:

- μ [-] — friction coefficient between tire and pavement surface.

During full-braking, both the vertical force $F_z = 5\ kN$ and longitudinal force $F_y = 4\ kN$ act on the tire rim. Figure 10 illustrates the distribution of tire contact stresses under full-braking. The tire contact area shows a shape similar to the free-rolling condition, but the intensity of the distribution of contact stresses differs. As a result of braking force action, the maximum contact stress area is concentrated along the negative y-axis.

Referring to Figures 10b and 10c, both vertical and transverse stresses of full-braking condition are very similar to those of free-rolling condition as there is no lateral force acting on the tire under two conditions. However, Figure 10d shows that the magnitude of longitudinal contact stress increases drastically in the full-braking condition in comparison with the free-rolling condition. Additionally, the longitudinal stresses are symmetric in free-rolling and go from a negative minimum to a positive maximum while they are exclusively negative in full-braking. The average ratio of peak vertical, lateral, and longitudinal contact stress values is about 1: 0.18: 0.37. The increment of tangential contact stresses

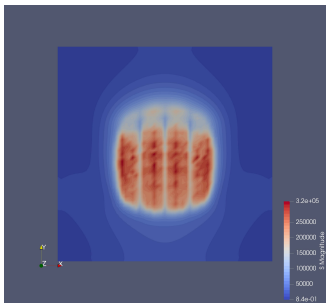

(a) Stress magnitude

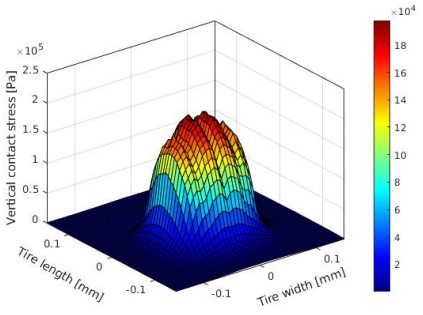

(b) Vertical contact stress

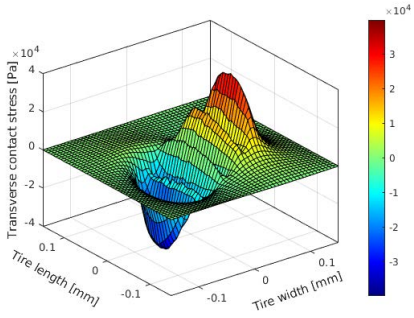

(c) Transverse contact stress

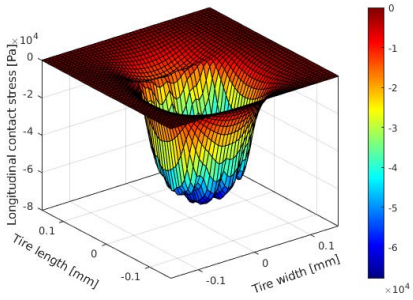

(d) Longitudinal contact stress

Figure 10: Contact stress distribution contour at full-braking

could accelerate the pavement surface deterioration.

5. Micro simulation of pavement response to the interaction with tire

5.1. Asphalt mixture modeling

The macro-scale model of the tire-pavement surface interaction above was used to study further the effect of various tire rolling conditions on pavement responses at the particle scale. This section describes the creation of a DEM pavement surface layer via CD method, the main work of the DEM modeling for asphalt mixtures is based on our previous work [49].

In an asphalt mixture, aggregates, bitumen and air are present simultaneously and aggregates weigh almost 95% of the mass. Consequently, from a geometrical point of view, asphalt mixture can be viewed as a system of irregular particle tessellations, and particles interact with each other through a viscoelastic mastic phase containing bitumen and air. The open-source software NEPER [53, 54] was adopted to generate tessellation samples of the surface layer based on the particle size distribution (PSD) (Table 1) and morphology properties.

The following steps were followed to generate the mixture sample: i) Tessellations were created following the aggregate morphology statistics and PSD cut at 2 mm to reduce the total quantity of particles in the sample, so that finer aggregates are included in the asphalt mastic; ii) The vertices of each tessellation were imported in LMGC90 to build numerical models. At this stage, particles were generated based on the convex hull of vertices from the tessellation; iii) Original particles from the net tessellation were shrunk by multiplying a correction factor in order to create gaps accommodating the mastic phase among particles. Figure 11 gives the generation process of an asphalt mixture sample for complex modulus tests based on two-point bending (2PB) configuration,

where rigid particles interact with each other through the viscoelastic asphalt mastic. The detailed description of the modeling can be found in a previous study [49].

Table 1: Particle size distribution (PSD) of asphalt mixture

Diameter (mm)	12.5	10	8	6.3	4	2	1	0.5	0.25	0.125	0.063
PSD (%)	100	90	75	58	44	31	20	15	12	9	6.5

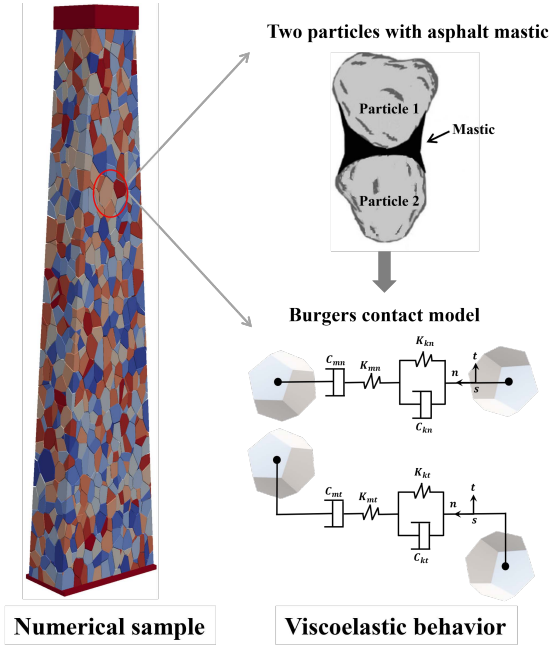

Figure 11: Numerical modeling of asphalt mixture for 2PB complex modulus test

Finally, the Burgers contact model was employed to simulate the viscoelastic behavior of asphalt mastic, more details about the numerical implementation of this contact model in CD method can be found elsewhere [55]. The normal and tangential properties of the Burgers contact model include stiffnesses and viscosities for the Maxwell and the Kelvin-Voigt parts, corresponding to K_{mi}, C_{mi}, K_{ki}, and C_{ki}, respectively, where i stands for n, t or s.

The normal components of the contact model can be determined by:

$$K_{mn} = A_c E_m / l_0 \tag{8}$$

$$C_{mn} = A_c \eta_m / l_0 \tag{9}$$

$$K_{kn} = A_c E_k / l_0 \tag{10}$$

$$C_{kn} = A_c \eta_k / l_0 \tag{11}$$

Where:

- E_m, η_m, E_k and η_k correspond to the macroscopic Maxwell and Kelvin-Voigt stiffnesses and viscosities respectively.
- A_c is the cross-section area of two particles in contact and l_0 is the initial distance between the particles.

Furthermore, the tangential components of the contact model for both tangential directions t and s can be derived from the above parameters, as:

$$K_{mt} = K_{ms} = \frac{K_{mn}}{2(1+\nu)} \tag{12}$$

$$C_{mt} = C_{ms} = \frac{C_{mn}}{2(1+\nu)} \tag{13}$$

$$K_{kt} = K_{ks} = \frac{K_{kn}}{2(1+\nu)} \tag{14}$$

$$C_{kt} = C_{ks} = \frac{C_{kn}}{2(1+\nu)} \tag{15}$$

Where:

- ν is the Poisson's ratio, it was set to 0.35 [55].

Regarding the experimental values for dynamic modulus $|E^*|$ and phase angle Φ for 15 °C, Figure 12 shows that numerical results are in good agreement with experimental measurements for $|E^*|$ and Φ for all the tested frequencies. The parameters for the Burgers contact model are listed in Table 2.

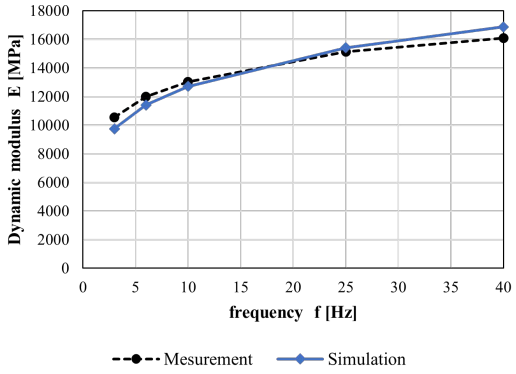

(a)

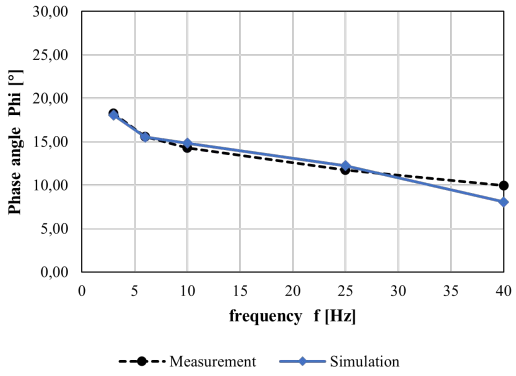

(b)

Figure 12: Dynamic modulus and phase angles from experimental measurements and simulations at 15°C: (a) Dynamic modulus; (b) Phase angle

Table 2: Burgers model parameters used in numerical simulations

Temperature ($°C$)	E_m (Pa)	η_m (Pa.s)	E_k (Pa)	η_k (Pa.s)
15	9.48×10^7	1.02×10^7	1.70×10^8	1.79×10^6

5.2. Non-uniform tire load simulation

Research about the simulation of non-uniform tire loads in DEM models is rare. Herein, we proposed a strategy to simulate non-uniform boundary conditions on the particle assembly inspired by previous studies of FEM simulations [56, 57]. When a tire is in motion on a pavement surface for a short period of time, the pavement surface, which is stiffer than the tire, almost retains its horizontal orientation during loading. Therefore, for a rolling tire in a steady-state, we applied directly the force field obtained from the contact stress distributions of the FEM tire model on the DEM asphalt layer surface. The coupling method allows for the computation to be efficiently solved while keeping accuracy, as it eliminates the massive contact detection between the tire elements and asphalt mixture particles and the internal calculation of the tire elements. Moreover, another advantage is that real particle shapes can be taken into account in the asphalt mixture simulation via DEM tools owing to the saving computation cost.

In the DEM model, the measured tire contact stresses (vertical, transverse, and longitudinal) under each rib were applied, respectively, on the tire contact area (Lx = 0.13 m, Ly = 0.22 m), as Figure 13 shows. By adjusting the number and size of elements within each rib, the exact shape of the tire contact patch at a given load level could be considered. Depending on their locations based on the tire contact area, all elements along a tire rib have varying contact stresses along with the vertical, longitudinal and lateral directions. For an accurate capture of tire contact stresses, in particular longitudinal contact stress, while conserving calculation efficiency, the element length and width were equal to the tire thread width and the groove gap, respectively. The contact stresses were converted to equivalent concentrated forces using element shape functions as implemented into the FEM calculations, and all forces were assumed constant

throughout the calculation.

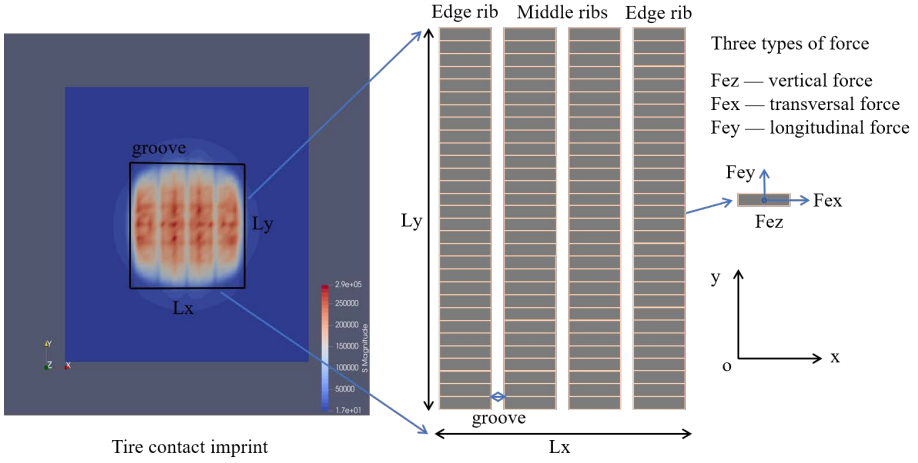

Figure 13: Tire imprint and contact stresses under each rib

Figure 14 displays a example of derived tire contact forces at free-rolling, it can be found that these boundary forces present a consistent distribution as the tire contact stresses aforementioned, which proves the method effectiveness.

After the mixture calibration describe in the previous part, we generated a pavement surface layer composed of polyhedral particles consistent with the tire contact dimensions (Figure 15a), where the bottom particles were fixed using a fixing boundary wall. Considering the viscoelastic contact between particles, the full pavement model comprised about 25,000 polyhedrons, leading to a large computation cost. As described before, the spatial distribution of tire contact stresses under both free-rolling and full braking is symmetrical along the longitudinal axis. Regarding the symmetrical boundary conditions, a symmetrical simulation strategy was adopted in the simulation in order to reduce the computational cost. The simulation only considers the half pavement model during the calculation, simultaneously, the freedom of x-direction for particles located on the center surface was fixed, as shown in Figure 15b. Finally, the tire loads were applied to the half pavement model as force boundary conditions, we stud-

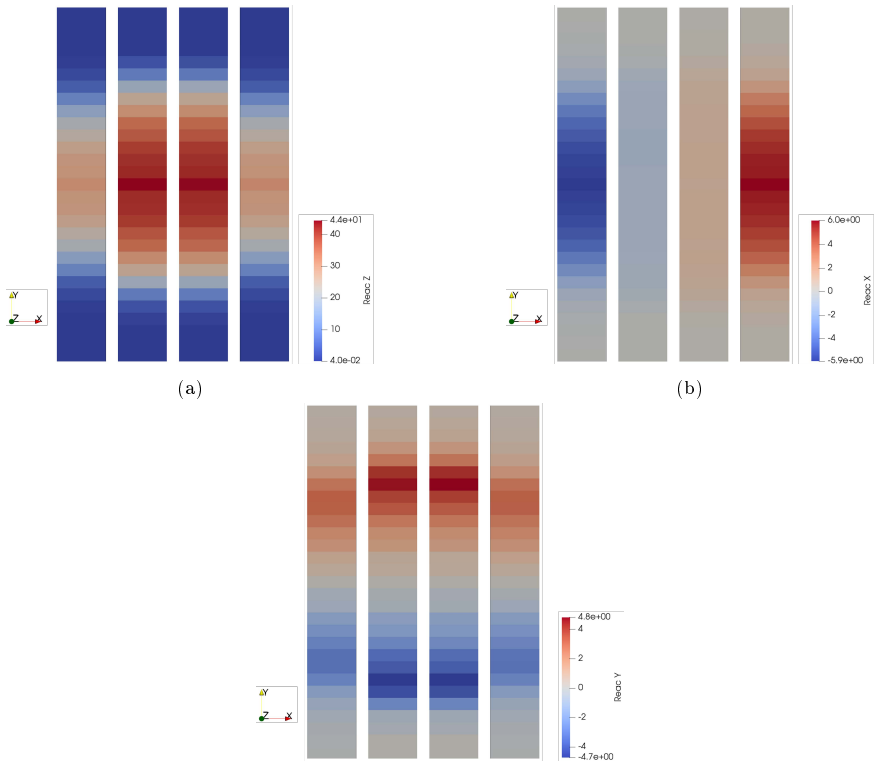

(a) (b)

(c)

Figure 14: Boundary forces derived from free-rolling (a) Vertical force (b) Longitudinal force (c) Transverse force

ied the pavement responses after a short loading time (1×10^{-2} s) in order to simulate an instantaneous dynamic loading.

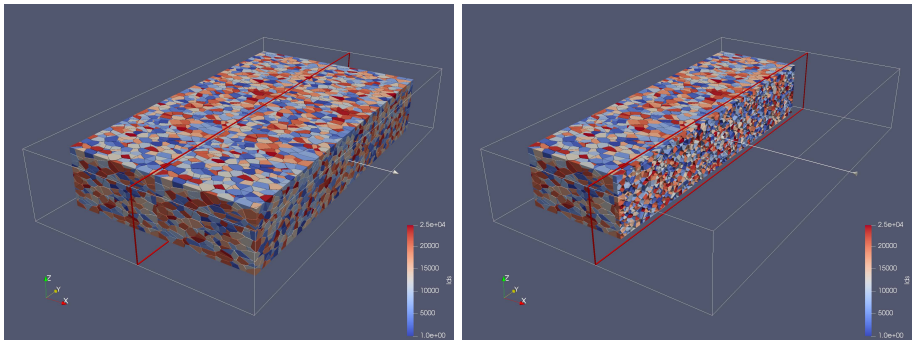

(a) (b)

Figure 15: Pavement surface layer model: (a) Full model; (b) Half model along y-axis

5.3. Particle displacement distribution

Figure 16a shows the particle displacement distribution under free-rolling condition. The arrows in the figure represent the particle moving direction, and the color of the arrows indicates the magnitude of the particle displacement. It can be seen that particle displacements distribute non-uniformly in the mixture, where particles near the center have larger displacements than those in other regions, which is consistent with the stress concentration under the free-rolling condition. In general, the arrow direction is essentially vertical since vertical contact stress dominates the entire tire contact stresses, whereas particles that lie under both sides have a horizontal component of particle displacement due to the existence of longitudinal and lateral contact stresses.

Figure 16b shows the particle displacement distribution under full-braking condition. The peak displacements appear concentrated on one side of the model along the longitudinal direction. Particles have an obvious longitudinal displacement component owing to the significant longitudinal contact stress. Note that particles under both free-rolling and full-braking conditions have a

similar lateral displacement distribution since the lateral tire contact stresses occur in a comparable pattern on the pavement surface for the two loading conditions.

Comparing the particle displacement distribution under free-rolling and full-braking conditions, the whole particle displacement under full-braking is larger than that under free-rolling. Figure 17 gives the comparison for peak values of the particle displacement and their components in the three directions under free-rolling and full-braking. Despite the similarities of their lateral components (x-direction) and vertical components (z-direction), the particle displacements are quite different along y-direction due to the differences in longitudinal tire contact stresses. Under full-braking loading, the displacement of particles becomes intensified, especially in the longitudinal direction. The strong boundary condition of contact stresses causes particles to rotate around the lateral direction, possibly leading to structural instability and high tensile strain and stress of the mixture.

5.4. Particle contact force analysis

At the contact plane between two particles, there are two main types of forces: the tangential force that induces shearing in the contact plane, and the normal force lying perpendicular to that plane. Both forces contribute to particle contacts being damaged, causing contact breakage and particle movement, leading to macro-cracks forming and propagating inside the mixture. Figure 18 shows the normal force distribution for particles subjected to free-rolling and full-braking conditions. The normal force values for full-braking and free-rolling conditions distribute asymmetrically along the y-axis (x=0), due to the fact that particles undergo mainly a compression state under both loading conditions owing to the vertical contact stresses and the normal force distributes primarily in one side of the axis.

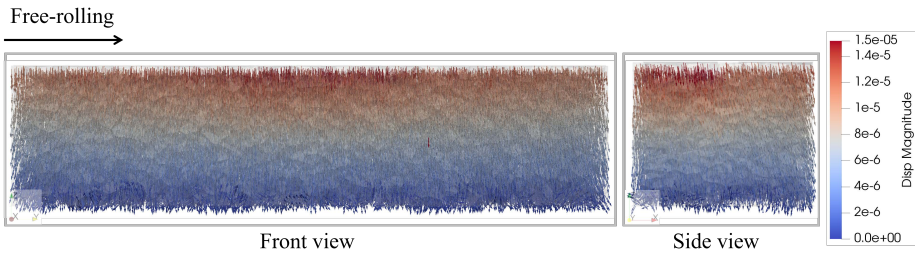

(a)

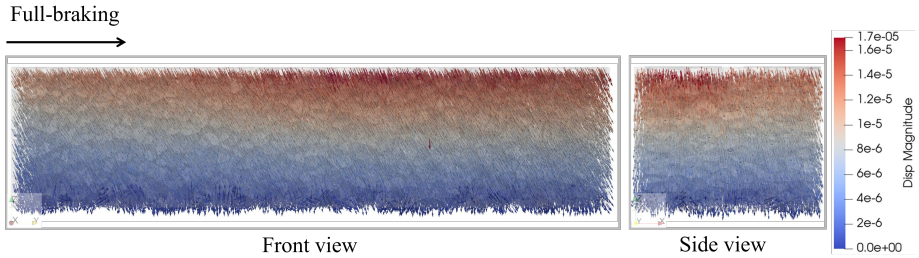

(b)

Figure 16: Particle displacement distribution under (a) free-rolling condition (b) full-braking condition

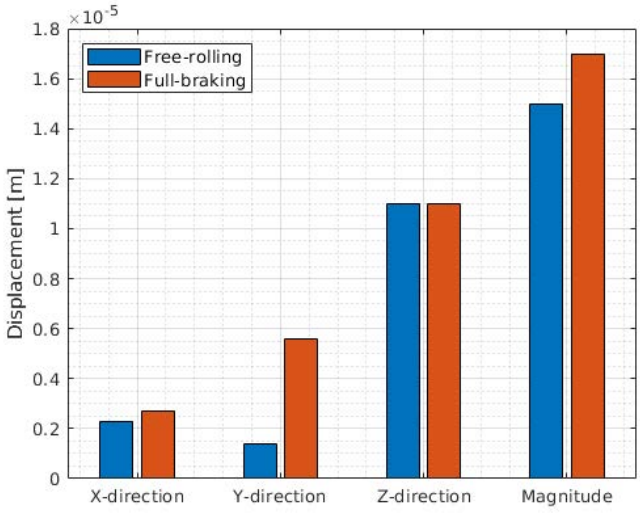

Figure 17: Maximum displacement comparison between free-rolling and full-braking

Figure 19 shows the distribution of tangential force values under different loading conditions. The tangential force values for both full-braking and free-rolling conditions follow approximately a normal distribution centered at zero. A larger magnitude range of tangential force values is observed under full-braking than that under free-rolling, which indicates that full-braking loading induces a stronger shear effect among particles than free-rolling loading, resulting in possible earlier damage initiation within the mixture.

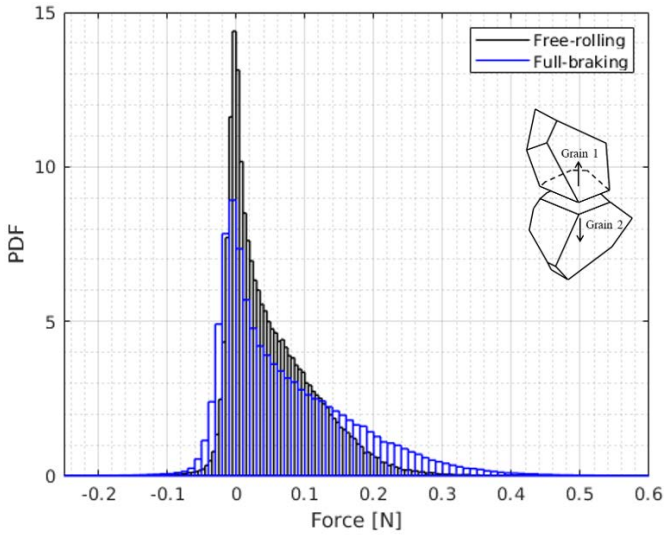

Figure 18: Normal force distribution

Pavement design methods traditionally consider only the vertical tire load and assume that the load is uniformly distributed. Nevertheless, based on the above multiscale analysis, these assumptions could be unreliable for investigating the degradation mechanisms of the asphalt pavement surface. The contact stresses distribute non-uniformly across the contact area; the tangential contact stresses caused by the tire are inevitable, particularly in acceleration or braking, which is crucial to the asphalt mixture responses. For predicting surface failures such as top-down cracks, taking only vertical contact stress into account

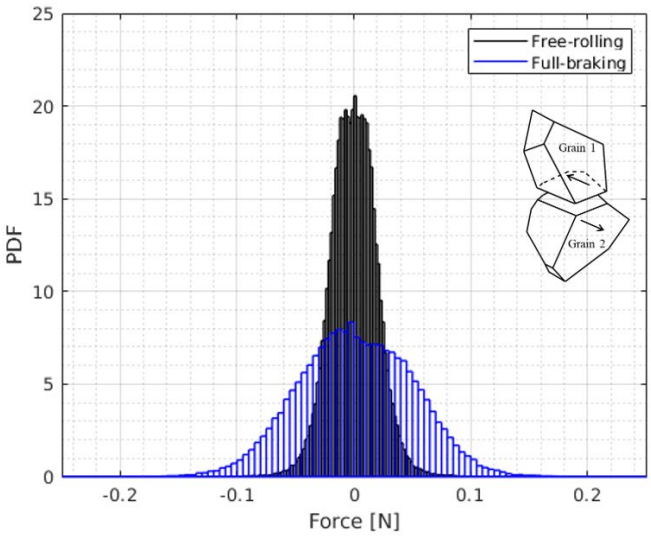

Figure 19: Tangential force distribution

and assuming uniform contact stress appears inadequate, as it could lead to misinterpretations of pavement responses under tire loading.

6. Conclusions

This study has introduced the CD method to conduct a multiscale FEM-DEM simulation for the tire-pavement interaction investigation. The main conclusions drawn are as follows:

(1) The CD method is introduced to enforce the contact condition between the tire and the pavement surface because of its performance in non-linear system simulation. The tire modeling strategy and its calibration were detailed. The tire geometry was reconstructed via laser scanning and image processing techniques. The tire structure was built by FEM according to its function and the relevant parameters were identified with a compression test.

(2) The contact stress distributions under free-rolling and full-braking reveal

that the tire induces contact stresses in three directions (vertical, transverse, longitudinal) and the contact stresses are not uniform across the contact area. The tangential contact stress on the pavement surface under full-braking is much higher than that under free-rolling.

(3) The internal mixture responses under tire loads were investigated by modeling a pavement surface layer via DEM. Under the full-braking condition, particle displacement distribution illustrates that particles tend to flow along the longitudinal direction and rotate ahead, which may lead to structural instability of the mixture. According to the analysis of particle contact forces, the tangential force values under full-braking have a wider distribution range than those under free rolling. It indicates that the full-braking condition induces a greater shear effect within particles in the mixture than the free-rolling condition, and may thereby result in earlier damage initiation.

(4) The proposed simulation method of the tire-pavement interaction incorporates the advantages that FEM can simulate contact stresses precisely on the asphalt pavement surface and DEM is capable of examining internal responses of the asphalt mixture at the particle scale. The present study combines FEM with DEM together to analyze pavement surface degradation under tire loads, which offers a promising way of optimizing pavement surface design.

Acknowledgements

The work presented in this paper was financially supported by the French National Research Agency (ANR-SolDuGri project ANR-14-CE22-0019). The first author gratefully acknowledge financial support from China Scholarship Council (No. 201806560055).

Conflict of interest

The authors declare that they have no conflict of interest.

References

[1] Y. H. Huang, et al., Pavement analysis and design (1993).

[2] J.-F. Corté, M.-T. Goux, Design of pavement structures: the french technical guide, Transportation research record 1539 (1) (1996) 116–124.

[3] H. L. Theyse, M. Muthen, Pavement analysis and design software (pads) based on the south african mechanistic-empirical design method, SATC 2000 (2000).

[4] M. Pau, B. Leban, A. Baldi, Ultrasonic measurements of contact area and pressure distribution of a pneumatic tire on a rigid surface, Tire Science and Technology 36 (1) (2008) 43–62.

[5] M. De Beer, C. Fisher, Stress-in-motion (sim) system for capturing triaxial tyre–road interaction in the contact patch, Measurement 46 (7) (2013) 2155–2173.

[6] H. Wang, I. L. Al-Qadi, Impact quantification of wide-base tire loading on secondary road flexible pavements, Journal of Transportation Engineering 137 (9) (2011) 630–639.

[7] D.-W. Park, E. Fernando, J. Leidy, Evaluation of predicted pavement response with measured tire contact stresses, Transportation Research Record 1919 (1) (2005) 160–170.

[8] R. V. Siddharthan, N. Krishnamenon, M. El-Mously, P. E. Sebaaly, Investigation of tire contact stress distributions on pavement response, Journal of Transportation Engineering 128 (2) (2002) 136–144.

[9] X. Jiang, C. Zeng, X. Gao, Z. Liu, Y. Qiu, 3d fem analysis of flexible base asphalt pavement structure under non-uniform tyre contact pressure, International Journal of Pavement Engineering 20 (9) (2019) 999–1011.

[10] I. L. Al-Qadi, H. Wang, P. J. Yoo, S. H. Dessouky, Dynamic analysis and in situ validation of perpetual pavement response to vehicular loading, Transportation Research Record 2087 (1) (2008) 29–39.

[11] H. Wang, I. L. Al-Qadi, I. Stanciulescu, Simulation of tyre–pavement interaction for predicting contact stresses at static and various rolling conditions, International Journal of Pavement Engineering 13 (4) (2012) 310–321.

[12] M. Guo, X. Zhou, Tire-pavement contact stress characteristics and critical slip ratio at multiple working conditions, Advances in Materials Science and Engineering 2019 (2019).

[13] M. Guo, X. Li, M. Ran, X. Zhou, Y. Yan, Analysis of contact stresses and rolling resistance of truck-bus tyres under different working conditions, Sustainability 12 (24) (2020) 10603.

[14] I. Wollny, R. Behnke, K. Villaret, M. Kaliske, Numerical modelling of tyre–pavement interaction phenomena: coupled structural investigations, Road Materials and Pavement Design 17 (3) (2016) 563–578.

[15] I. Wollny, F. Hartung, M. Kaliske, P. Liu, M. Oeser, D. Wang, G. Canon Falla, S. Leischner, F. Wellner, Coupling of microstructural and macrostructural computational approaches for asphalt pavements under rolling tire load, Computer-Aided Civil and Infrastructure Engineering 35 (11) (2020) 1178–1193.

[16] E. Manyo, P. Reynaud, B. Picoux, R. Tautou, F. Allou, C. Petit, D. Nélias, Tire–pavement tractive rolling contact under turning conditions: towards

pavement top-down cracking, International Journal of Pavement Engineering (2020) 1–10.

[17] E. Y. Manyo, B. Picoux, P. Reynaud, R. Tautou, D. Nelias, F. Allou, C. Petit, Approach of pavement surface layer degradation caused by tire contact using semi-analytical model, Materials 14 (9) (2021) 2117.

[18] Y. Oubahdou, E. Wallace, P. Reynaud, B. Picoux, J. Dopeux, C. Petit, D. Nélias, Effect of the tire–pavement contact at the surface layer when the tire is tilted in bend, Construction and Building Materials 305 (2021) 124765.

[19] W. G. Buttlar, Z. You, Discrete element modeling of asphalt concrete: microfabric approach, Transportation Research Record 1757 (1) (2001) 111–118.

[20] Y. Liu, Q. Dai, Z. You, Viscoelastic model for discrete element simulation of asphalt mixtures, Journal of Engineering Mechanics 135 (4) (2009) 324–333.

[21] A. Collop, G. McDowell, Y. Lee, On the use of discrete element modelling to simulate the viscoelastic deformation behaviour of an idealized asphalt mixture, Geomechanics and Geoengineering: An International Journal 2 (2) (2007) 77–86.

[22] G. Dondi, V. Vignali, M. Pettinari, F. Mazzotta, A. Simone, C. Sangiorgi, Modeling the dsr complex shear modulus of asphalt binder using 3d discrete element approach, Construction and building Materials 54 (2014) 236–246.

[23] Z. You, W. G. Buttlar, Application of discrete element modeling techniques to predict the complex modulus of asphalt–aggregate hollow cylinders sub-

jected to internal pressure, Transportation Research Record 1929 (1) (2005) 218–226.

[24] Z. You, S. Adhikari, M. E. Kutay, Dynamic modulus simulation of the asphalt concrete using the x-ray computed tomography images, Materials and Structures 42 (5) (2009) 617–630.

[25] T. Ma, H. Wang, D. Zhang, Y. Zhang, Heterogeneity effect of mechanical property on creep behavior of asphalt mixture based on micromechanical modeling and virtual creep test, Mechanics of Materials 104 (2017) 49–59.

[26] J. Chen, B. Huang, F. Chen, X. Shu, Application of discrete element method to superpave gyratory compaction, Road materials and pavement design 13 (3) (2012) 480–500.

[27] F. Gong, X. Zhou, Z. You, Y. Liu, S. Chen, Using discrete element models to track movement of coarse aggregates during compaction of asphalt mixture, Construction and Building Materials 189 (2018) 338–351.

[28] T. Ma, D. Zhang, Y. Zhang, J. Hong, Micromechanical response of aggregate skeleton within asphalt mixture based on virtual simulation of wheel tracking test, Construction and Building Materials 111 (2016) 153–163.

[29] T. Ma, D. Zhang, Y. Zhang, S. Wang, X. Huang, Simulation of wheel tracking test for asphalt mixture using discrete element modelling, Road Materials and Pavement Design 19 (2) (2018) 367–384.

[30] B. Xue, J. Xu, J. Pei, J. Zhang, R. Li, Investigation on the micromechanical response of asphalt mixture during permanent deformation based on 3d virtual wheel tracking test, Construction and Building Materials 267 (2021) 121031.

[31] H. Wang, Z. Zhou, W. Huang, X. Dong, Investigation of asphalt mixture permanent deformation based on three-dimensional discrete element method, Construction and Building Materials 272 (2021) 121808.

[32] H. Yamashita, G. Chen, Y. Ruan, P. Jayakumar, H. Sugiyama, Hierarchical multiscale modeling of tire–soil interaction for off-road mobility simulation, Journal of Computational and Nonlinear Dynamics 14 (6) (2019).

[33] M. Michael, F. Vogel, B. Peters, Dem–fem coupling simulations of the interactions between a tire tread and granular terrain, Computer Methods in Applied Mechanics and Engineering 289 (2015) 227–248.

[34] C.-L. Zhao, M.-Y. Zang, Application of the fem/dem and alternately moving road method to the simulation of tire-sand interactions, Journal of Terramechanics 72 (2017) 27–38.

[35] P. Wriggers, G. Zavarise, Computational contact mechanics, Encyclopedia of computational mechanics (2004).

[36] P. A. CUNDALL, A computer model for simulating progressive, large-scale movement in blocky rock system, Proceedings of the International Symposium on Rock Mechanics, 1971 (1971).
URL https://ci.nii.ac.jp/naid/10018723276/en/

[37] P. A. Cundall, O. D. Strack, A discrete numerical model for granular assemblies, geotechnique 29 (1) (1979) 47–65.

[38] M. Jean, J. J. Moreau, Dynamics in the presence of unilateral contacts and dry friction: A numerical approach, in: G. Del Piero, F. Maceri (Eds.), Unilateral Problems in Structural Analysis — 2, Springer Vienna, Vienna, 1987, pp. 151–196.

[39] M. Jean, The non-smooth contact dynamics method, Computer methods in applied mechanics and engineering 177 (3-4) (1999) 235–257.

[40] J. J. Moreau, Unilateral contact and dry friction in finite freedom dynamics, in: Nonsmooth mechanics and Applications, Springer, 1988, pp. 1–82.

[41] F. Dubois, V. Acary, M. Jean, The contact dynamics method: A nonsmooth story, Comptes Rendus Mécanique 346 (3) (2018) 247–262.

[42] F. Radjai, V. Richefeu, Contact dynamics as a nonsmooth discrete element method, Mechanics of Materials 41 (6) (2009) 715–728.

[43] P. A. Cundall, Formulation of a three-dimensional distinct element model—part i. a scheme to detect and represent contacts in a system composed of many polyhedral blocks, in: International Journal of Rock Mechanics and Mining Sciences & Geomechanics Abstracts, Vol. 25, Elsevier, 1988, pp. 107–116.

[44] E. G. Nezami, Y. M. Hashash, D. Zhao, J. Ghaboussi, A fast contact detection algorithm for 3-d discrete element method, Computers and Geotechnics 31 (7) (2004) 575–587.

[45] E. G. Nezami, Y. MA Hashash, D. Zhao, J. Ghaboussi, Shortest link method for contact detection in discrete element method, International Journal for Numerical and Analytical Methods in Geomechanics 30 (8) (2006) 783–801.

[46] H. Yamashita, Flexible multibody dynamics approach for tire dynamics simulation, Ph.D. thesis, University of Iowa (2016). doi:10.17077/etd.gfixb2od.
URL https://ir.uiowa.edu/etd/2297

[47] E. Y. Manyo, P. Reynaud, B. Picoux, R. Tautou, D. Nelias, F. Allou, C. Petit, Towards fast modelling of the tire-pavement contact, European Journal of Environmental and Civil Engineering (2019) 1–17.

[48] K. L. Johnson, Contact Mechanics, Cambridge University Press, 1985. doi:10.1017/CBO9781139171731.

[49] H. Ge, J. C. Quezada, V. L. Houerou, C. Chazallon, Three-dimensional simulation of asphalt mixture incorporating aggregate size and morphology distribution based on contact dynamics method, Construction and Building Materials 302 (2021) 124124. doi:https://doi.org/10.1016/j.conbuildmat.2021.124124.
URL https://www.sciencedirect.com/science/article/pii/S0950061821018845

[50] C. EN, et al., Bituminous mixtures–test methods for hot mix asphalt–part 26: Stiffness (2012).

[51] H. Pacejka, Tire and vehicle dynamicss, 2nd ed., Butterworth-Heinemann, Oxford, UK, 2006, 2005.

[52] Y. Xiong, In-plane Tire Deformation Measurement Using a Multi-Laser Sensor System, Doctoral thesis, School of Engineering (2016).
URL http://urn.fi/URN:ISBN:978-952-60-6803-9

[53] R. Quey, P. Dawson, F. Barbe, Large-scale 3d random polycrystals for the finite element method: Generation, meshing and remeshing, Computer Methods in Applied Mechanics and Engineering 200 (17-20) (2011) 1729–1745.

[54] R. Quey, L. Renversade, Optimal polyhedral description of 3d polycrystals: method and application to statistical and synchrotron x-ray diffrac-

tion data, Computer Methods in Applied Mechanics and Engineering 330 (2018) 308–333.

[55] J. C. Quezada, C. Chazallon, Complex modulus modeling of asphalt concrete mixes using the non-smooth contact dynamics method, Computers and Geotechnics 117 (2020) 103255.

[56] H. Wang, H. Ozer, I. L. Al-Qadi, C. A. Duarte, Analysis of near-surface cracking under critical loading conditions using uncracked and cracked pavement models, Journal of transportation engineering 139 (10) (2013) 992–1000.

[57] Z. Dong, X. Ma, Analytical solutions of asphalt pavement responses under moving loads with arbitrary non-uniform tire contact pressure and irregular tire imprint, Road Materials and Pavement Design 19 (8) (2018) 1887–1903.

Tire compression test

Tire contact force derivation

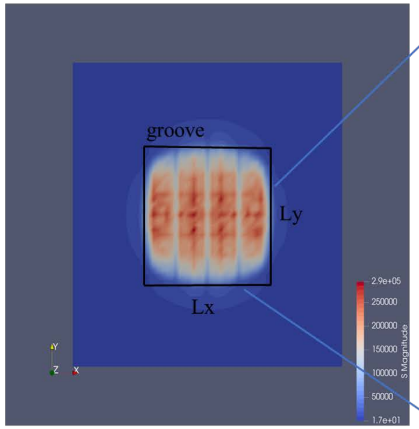

Asphalt layer modeling

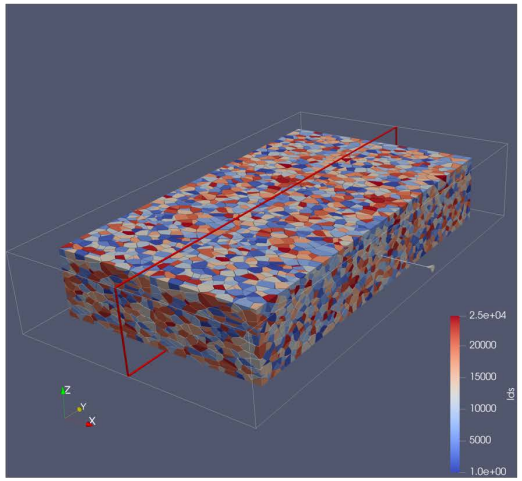

Asphalt mixture calibration

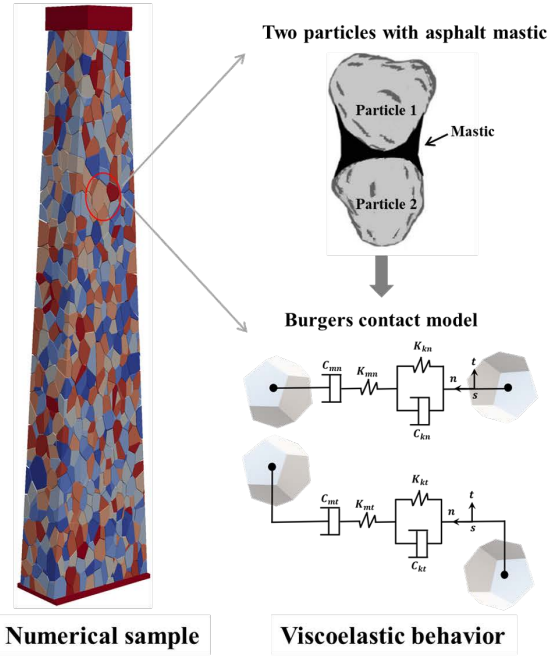

Numerical anaylis